Title

Spontaneous dark formation of OH radicals at the interface of aqueous atmospheric droplets.

Journal

Proceedings of the National Academy of Sciences of USA, 120(15)

Authors

Rudich, Yinon
Angelaki, Maria
Wang, Xinke
et al.

Publication Date

2023-04-11

DOI

10.1073/pnas.2220228120

Peer reviewed

PNAS RESEARCH ARTICLE | EARTH, ATMOSPHERIC, AND PLANETARY SCIENCES

Spontaneous dark formation of OH radicals at the interface of aqueous atmospheric droplets

Kangwei Li[a,1], Yunlong Guo[a,b], Sergey A. Nizkorodov[c], Yinon Rudich[d], Maria Angelaki[a], Xinke Wang[c], Taicheng An[b], Sebastien Perrier[a], and Christian George[a,2]

Edited by Mark Thiemens, University of California San Diego, La Jolla, CA; received November 28, 2022; accepted March 10, 2023

Hydroxyl radical (OH) is a key oxidant that triggers atmospheric oxidation chemistry in both gas and aqueous phases. The current understanding of its aqueous sources is mainly based on known bulk (photo)chemical processes, uptake from gaseous OH, or related to interfacial O_3 and NO_3 radical-driven chemistry. Here, we present experimental evidence that OH radicals are spontaneously produced at the air–water interface of aqueous droplets in the dark and the absence of known precursors, possibly due to the strong electric field that forms at such interfaces. The measured OH production rates in atmospherically relevant droplets are comparable to or significantly higher than those from known aqueous bulk sources, especially in the dark. As aqueous droplets are ubiquitous in the troposphere, this interfacial source of OH radicals should significantly impact atmospheric multiphase oxidation chemistry, with substantial implications on air quality, climate, and health.

air–water interface | OH radicals | atmospheric chemistry | aqueous microdroplets

Significance

Recent studies suggest that reactions that do not usually occur in bulk solution can occur spontaneously in small water droplets, possibly due to the naturally formed electric field at the air–water interface. We explore the atmospheric significance of this process by demonstrating efficient spontaneous production of interfacial hydroxyl radicals (OH) from aqueous droplets under ambient conditions. This interfacial OH production does not involve precursors or catalysts, such as light or heat, and is likely the largest aqueous OH source in atmospheric droplets at nighttime. The ubiquity of aqueous aerosols and cloud droplets and their possibly strong OH-producing capability suggests that we have to rethink atmospheric multiphase oxidation chemistry.

Water is the most common liquid on Earth and is stable and inert under ambient conditions. Its ubiquitous presence in the environment creates a large number of air–water interfaces of various sizes, ranging from the surface of oceans or lakes to (sub)micron-sized aerosols, fog, and cloud droplets with high surface-to-volume ratios (1–4). Atmospheric aerosol droplets have a particular importance due to their roles in occurrences of severe air pollution (5) with adverse effects on human health (6) as well as their direct and indirect impacts on Earth's climate (7, 8). Very recently, some unique physical and chemical properties have been found at the air–water interface of microdroplets, which could accelerate chemical reactions (9), and trigger spontaneous degradation of organic compounds and spontaneous H_2O_2 formation (10–13). While the underlying mechanism of such high surface reactivity is still debated, it is likely driven by the localized high electric field ($\sim 10^9$ V m^{-1}) that forms at the aqueous interface (14, 15). A few decades ago, while examining the energetics and thermodynamics of water, Kloss (16) suggested that a minor fraction of hydroxide anion exists as a radical–electron pair (OH and e^-), which may reversibly dissociate into an OH radical and an electron (e^-) when it is subject to an external perturbation such as an electric field in pure water. For instance, water splitting or electrolysis of water, which is a different process than the one discussed here, produces hydrogen and requires a minimum potential difference of 1.23 V (17), which is of the same order of magnitude as the one observed at the air–water interface. The OH radicals produced by the radical–electron pair dissociation may recombine to generate H_2O_2. These theoretical speculations are supported by recent observations (10, 11, 18) and theoretical calculation (19) of spontaneous H_2O_2 formation in micron-sized and condensing droplets, where the formation of peroxide is regarded as the evidence for OH radical generation at the interface (20, 21). It is worth mentioning that OH production has also been discussed in the context of the interfacial chemistry of phenolic compounds exposed to gaseous O_3 and NO_3 radicals, as explored by online electrospray ionization mass spectrometry (22–25).

In the context of atmospheric chemistry, the presence of aqueous-phase $OH_{(aq)}$ radicals is attributed to uptake from the gas phase or to in situ production by (photo)chemical reactions (26), such as photolysis of H_2O_2, NO_3^-, NO_2^-, and Fenton or photo-Fenton reactions (27, 28). However, the sources and sinks of $OH_{(aq)}$ radicals are still not fully constrained, resulting in significant uncertainties in model simulations for sulfate and organic component formation in aqueous aerosol and cloud droplets (29, 30), which underlines our current incomplete understanding of atmospheric oxidation chemistry. In addition, other recent studies (22–25) have also observed the generation of OH radicals during the oxidation of phenolic compounds via gas-phase O_3 and NO_3 radicals at the air–water interface. Our understanding of the underlying physical and chemical processes in these experiments can only be achieved through properly designed laboratory investigations as noted by Pillar-Little and Guzman (31).

Author contributions: K.L., S.A.N., Y.R., X.W., S.P., and C.G. designed research; K.L., Y.G., M.A., and S.P. performed research; K.L., Y.G., S.A.N., Y.R., X.W., S.P., and C.G. analyzed data; and K.L., Y.G., S.A.N., Y.R., X.W., T.A., S.P., and C.G. wrote the paper.

The authors declare no competing interest.

This article is a PNAS Direct Submission.

[1]Present address: Department of Environmental Sciences, University of Basel, Basel 4056, Switzerland.

[2]To whom correspondence may be addressed. Email: christian.george@ircelyon.univ-lyon1.fr.

This article contains supporting information online at https://www.pnas.org/lookup/suppl/doi:10.1073/pnas.2220228120/-/DCSupplemental.

Published April 3, 2023.

Using different experimental approaches, we investigated whether OH radicals may be spontaneously generated at the air–water interface of water droplets under ambient atmospheric conditions. None of these experiments involves any known OH precursor (i.e., Fe(II) cations for Fenton-type reactions) or catalysts such as light or heat. We demonstrate that this spontaneous interfacial production competes with the OH flux taken up from the gas phase and is more significant than known bulk chemical sources. It may dominate the aqueous-phase OH production and atmospheric transformations during nighttime.

Results and Discussion

Confirmation of $OH_{(aq)}$ Production at the Air–Water Interface. The tiny concentrations of $OH_{(aq)}$ present in environmental systems make this species extremely challenging to measure directly under most conditions. Therefore, we used a chemical titrant and proceeded with an indirect determination. Both terephthalic acid and disodium terephthalate (TA) have been previously used as a probe for in situ quantification of $OH_{(aq)}$ radicals that form in bulk solutions (32–35) and at the air–water interface of microdroplets (23). Since terephthalic acid has low solubility in water, we used disodium terephthalate(TA) (*SI Appendix*, Text S1) to overcome the solubility issue for the whole study. This reaction produces a fluorescent product, namely 2-hydroxyterephthalic acid (TAOH), with a yield of 0.315 (33) (Fig. 1*A*). The TAOH thus produced can be quantified through fluorescence spectroscopy with high sensitivity (detection limit at ~0.5 nM), making it possible to quantify the OH production rate (*SI Appendix*, Figs. S1 and S2 and Text S2).

First, we investigated whether interfacial production occurs on flat macroscopic water surfaces by either fully (i.e., with no headspace) or partially filled (with only 3 mL, thereby creating an air–water interface with a known surface area) 60-mL glass bottles with TA solution and allowing them to stand for several weeks in

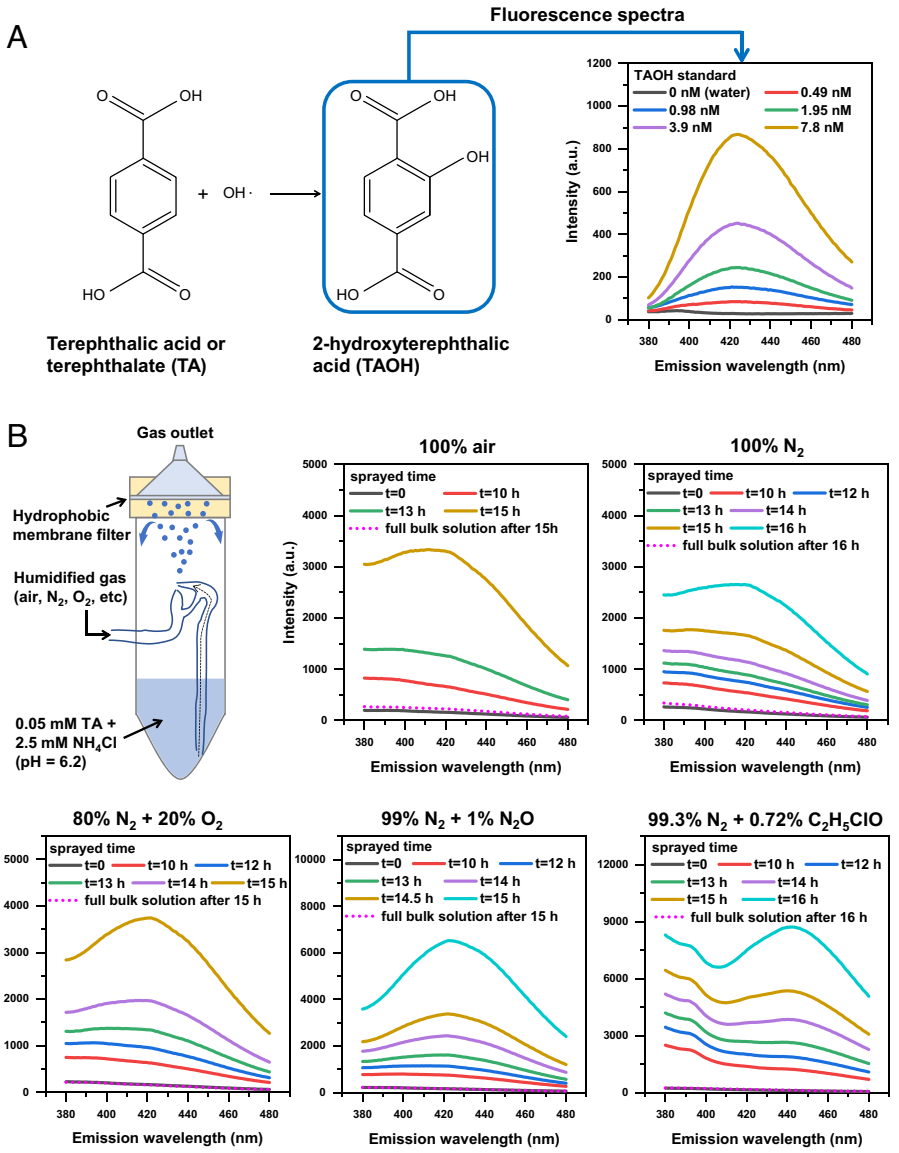

Fig. 1. Confirmation of $OH_{(aq)}$ production at the air–water interface of microdroplets. (*A*) Aqueous reaction scheme between TA and $OH_{(aq)}$ radical forms fluorescent TAOH and typical fluorescence emission spectra (excited at 310 nm) of TAOH standards peaking at ~422 nm. (*B*) Schematic of the home-built mist chamber for spraying TA-containing droplets, where the bulk TA solution was naturally lifted up and sprayed out when introducing humidified gases to create a pressure differential (Video S1). Time-dependent TAOH fluorescence emission spectra for the mist chamber solution (0.05 mM TA + 2.5 mM NH_4Cl, pH = 6.2, initially 20 mL) were obtained during 15 or 16 h spraying under five different gases, including pure air, pure N_2, and N_2 with added electron scavengers such as O_2, N_2O, and gaseous 2-chloroethanol (C_2H_5ClO), during which the produced microdroplets were prevented from escaping by the hydrophobic filter and maintained spraying and recycling overtime, and TAOH concentration was expected to accumulate in the bulk solution.

the dark (*SI Appendix*, Fig. S3 and Text S3). TAOH, and hence OH production, was only observed in the small-volume solutions, that is, only in the presence of an air–water interface, while no TAOH was observed in full bulk solution. This observation also unambiguously confirms that TAOH production is not related to any impurities present in the water used here.

To extend this result to aqueous droplets, we used a home-built glass-only mist chamber to produce microdroplets by gently spraying bulk solutions containing 0.05 mM TA + 2.5 mM NH_4Cl at pH = 6.2 under the action of a flow of pure air, pure nitrogen, or nitrogen mixed with gas-phase electron scavengers such as O_2, N_2O, and 2-chloroethanol (Fig. 1*B* and *SI Appendix*, Text S4). The addition of NH_4Cl into TA solution can enhance the ionic strength in spraying droplets that are comparable to atmospheric droplets (36) while maintaining a chemically inert and deliquesced state due to its well-known chemical and hygroscopic property. The interfacial surface area is increased by orders of magnitude higher in the droplets compared to a flat surface, thus increasing the potential for interfacial reactions to occur in a shorter time. The mist chamber was used in a recirculation mode, where droplets continuously impacted a membrane filter and dropped back into the bulk liquid before being resprayed into the headspace. We observed a clear formation of ~30 nM TAOH after 15 h of recycling using pure air as the bubbling gas. In comparison, no TAOH was observed for the same full bulk solution after 15 h with no air–water interface (Fig. 1*B*), providing further evidence for an interfacial production of OH radicals. The shorter timescale for product formation compared to the flat surface experiments reinforces that the surface area exposed to the air is a key factor for such interfacial processes.

Less TAOH was formed when using nitrogen as the spraying gas than was formed using clean air (Fig. 1*B* and *SI Appendix*, Fig. S4). Similar reduced TAOH formation under nitrogen was also observed from TA-containing microdroplets produced by a commercial atomizer (*SI Appendix*, Fig. S5 and Text S5), suggesting that our observation of TAOH formation from microdroplets does not depend on the spraying procedure. The following reaction scheme may explain the dependence of radical production on the carrier gas used:

$$OH^- \overset{electric\ field}{\rightleftharpoons} OH\bullet + e^-, \qquad [\mathbf{R1}]$$

$$O_2 + e^- \rightarrow O_2^-, \qquad [\mathbf{R2}]$$

$$O_2^- + H^+ \rightleftharpoons HO_2\bullet, \qquad [\mathbf{R3}]$$

$$HO_2\bullet + HO_2\bullet \rightarrow H_2O_2 + O_2, \qquad [\mathbf{R4}]$$

where $OH_{(aq)}$ and e^- are produced under the action of an electric field (16) (**R1**), followed by **R2**–**R4**, where the free electrons (e^-) are scavenged by dissolved oxygen, producing O_2^- and HO_2 radicals which self-react to produce H_2O_2. Under a pure nitrogen atmosphere, the solvated electron generated in **R1** can recombine fast with the nearby $OH_{(aq)}$ radicals due to cage effects, creating a null cycle. In contrast, we observed enhanced formation of TAOH when an electron scavenger such as O_2, N_2O, and 2-chloroethanol was added to the pure nitrogen gas spraying flow (Fig. 1*B* and *SI Appendix*, Fig. S4), supporting this proposed reaction scheme. The strength of such electric field, that forms naturally at the interface of microdroplets, was previously determined to be at the order of 10^9 V m^{-1} (14, 15), and the feasibility of this reaction (**R1**) has been examined by a recent theoretical simulation (19) in addition to the approach used by Kloss (16). This reaction scheme gives a plausible alternative explanation for the observed H_2O_2 formation by Lee et al. (10, 11) and less H_2O_2 formation in nitrogen compared to pure air (18).

$OH_{(aq)}$ Production in Submicron Aerosol Droplets. To better simulate atmospheric conditions with longer reaction time, smaller droplet concentrations, and smaller droplet diameters, TA-containing aerosol droplets from the atomizer output were directed into an atmospheric simulation chamber (~2 m^3), where the droplets have a lifetime of up to several hours. After injection, submicron droplets were periodically sampled from the chamber onto quartz filters and extracted with ultrapure water for subsequent chemical analysis. Noticeably, TA would become significantly concentrated, with a measured concentration of 400 ± 177 mM (average from n = 17 filters analyzed by LC-MS; see *SI Appendix*, Table S1 and Text S10) in submicron droplets after atomizing from the bulk 1 mM TA solution. To avoid any memory effect and impurities, the inner surface of the Teflon chamber was fully cleaned (scrubbed) with pure water and ethanol prior to starting these chamber experiments, and no residual NO_2 or O_3 was detectable (<0.5 ppb). The chamber was also kept at positive pressure to avoid diffusion of pollutants form the laboratory air.

Fig. 2 shows that the measured TAOH concentration reached ~1.3 mM in submicron droplets at pH = 6.5. This concentration of TAOH in submicron droplets is about four orders higher than the concentration in microdroplets directly measured at the atomizer output through condensing collection in the glass vessel (*SI Appendix*, Fig. S5). Such difference can be explained by 1) significantly smaller sizes of droplets injected into the chamber with a higher surface-to-volume ratio, 2) underestimated TAOH concentration measured at the atomizer output due to unaccounted dilution effect as both water vapor and microdroplets were condensed together, and 3) large residence time difference between submicron aerosol droplets in the chamber and microdroplets in a glass vessel (i.e., several hours vs. 1 to 2 min). Taking the aerosol residence time in the chamber into consideration, this yields a TAOH production rate of ~10 μM min^{-1} and hence an $OH_{(aq)}$ production rate of ca. 30 μM min^{-1} for submicron droplets (*SI Appendix*, Text S10). As shown in Fig. 2, some significant uncertainty is associated with these measurements, which are related to the varying droplet size distribution between different chamber experiments (*SI Appendix*, Table S1). It is expected that the spontaneous interfacial OH production is strongly size dependent, and further investigations with size-selected monodisperse droplets might reduce such uncertainty.

Measurements of pH of atmospheric droplets are difficult and usually estimated by thermodynamic models ranging from −1 to 5 for aerosols and from 2 to 7 for fog/cloud droplets (37). According to Eugene et al. (38), we assume that the pH of the produced TA-containing droplets is the same as the original bulk TA solution, and thus, the submicron droplets produced from weakly acidic bulk solution (pH = 5.0 or 6.5) should be within the atmospherically relevant pH range. Compared with alkaline solutions (pH = 9.0), weakly acidic (pH = 5.0 or 6.5) submicron droplets were associated with a higher TAOH production rate, consistent with the observations made at the atomizer output (*SI Appendix*, Fig. S5*D*). However, the pH dependence of interfacial OH production remains unexplained and requires more investigation in the future.

As a further test for the production of $OH_{(aq)}$, we added 3 mM or 10 mM adipic acid to our solutions as an $OH_{(aq)}$ scavenger, and aerosol droplets containing both TA and adipic acid were introduced

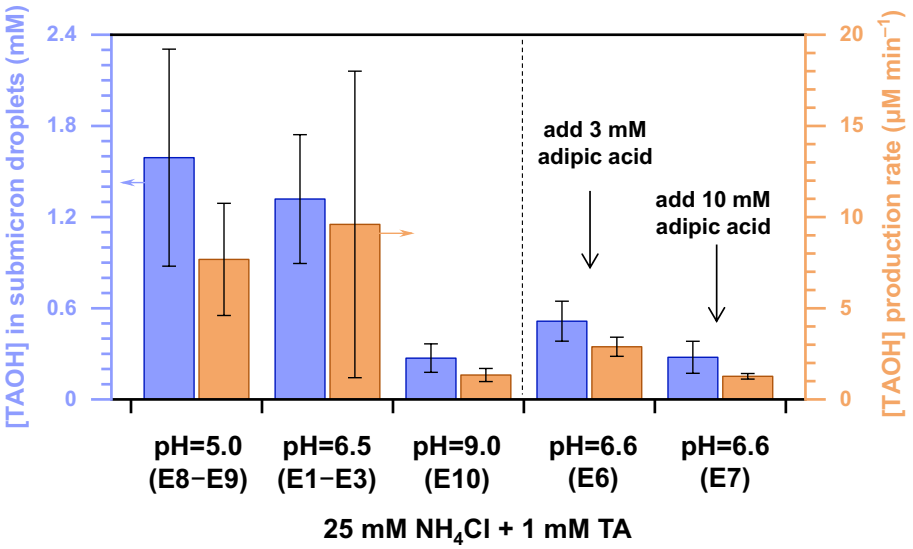

Fig. 2. Quantification of $OH_{(aq)}$ production in submicron aerosol droplets. The TAOH concentration and its production rate in submicron droplets were determined from chamber experiments. The TA-containing aerosol droplets were produced by atomizing 25 mM NH_4Cl + 1 mM TA solution at a different solution pH or by adding adipic acid (see *SI Appendix*, Table S1 for a detailed description of E1-E10 (as experiment ID).

into the chamber in the dark. Fig. 2 shows that lower TAOH concentrations were observed with increasing adipic acid concentration due to the chemical competition between TA and adipic acid for $OH_{(aq)}$ radicals. In addition, ketoadipic acid was observed as a reaction product in these experiments by using high-resolution LC-MS measurements (*SI Appendix*, Figs. S11 and S12) in agreement with the known chemistry of adipic acid with $OH_{(aq)}$ radicals (39). This is another indication that $OH_{(aq)}$ radicals are produced and can participate in condensed-phase chemistry.

Gas-Phase Compounds Oxidized by Interfacial OH Radical. Finally, we tested whether interfacial OH radicals produced from aerosol droplets can induce secondary oxidation chemistry for gas-phase species. For this purpose, we added ca. 1.1 ppm of cyclohexane vapor to the chamber. Cyclohexane is widely used as a gas-phase $OH_{(g)}$ scavenger with cyclohexanone and cyclohexanol as the major $OH_{(g)}$ oxidation products (40). If cyclohexane oxidation chemistry occurs, one would expect an increase in these oxidation products upon aqueous droplet injection into the chamber. As shown by Fig. 3, the mass signals of cyclohexanone and cyclohexanol (using Vocus - Proton Transfer Reaction – Time of Flight - Mass Spectrometry (PTR-ToF-MS) detection; see *SI Appendix*, Texts S8 and S9) increase immediately after introducing deliquesced NH_4HSO_4 aerosols into the chamber under dark conditions and then plateauing for ca. 4 to 5 h before decaying. This time evolution can be explained by interfacial OH production from the aerosol droplets, followed by cyclohexane oxidation to form these products, and then, wall losses in a chamber continuously flushed to compensate for the air flow from the various instruments connected to it (thereby inducing some dilution effect).

We note that the cyclohexanone signal in Fig. 3 also increased immediately during cyclohexane injection due to an instrument measurement interference from cyclohexane or impurity in cyclohexane vapor. We also notice the fast decay of cyclohexane after its injection into the chamber, and this decay does not change obviously in the presence of aerosol droplets or additional $OH_{(g)}$ produced under UV light (Fig. 3 and *SI Appendix*, Fig. S14). Therefore, the observed cyclohexane decay can be attributed to continuous dilution during the chamber experiments.

There are two plausible interpretations for the observed oxidation products upon aqueous droplet injection into the chamber: 1) gas-phase cyclohexane constantly collided with the droplet surface, with these products forming at the air–water interface the aerosol droplets, and 2) interfacial OH radicals desorb from the droplet surface and releasing into the gas phase as $OH_{(g)}$ and then reacted with cyclohexane in the gas phase. Note that the uptake of gas-phase cyclohexane into droplets is highly unlikely due to its low solubility in water. Although currently we cannot distinguish between these two possibilities, the observation of cyclohexane oxidation products in the gas phase serves as additional strong evidence for this spontaneous interfacial OH production, which can induce further oxidation chemistry for gas-phase compounds. However, more in-depth investigations on oxidation of gas-phase compounds by interfacial OH radical are still needed in the future, such as replacement of cyclohexane with other reactive compounds or quantification for these gaseous oxidation products.

Atmospheric Importance of Interfacial OH Radical Production. Previous studies (14, 15) showed experimental and theoretical evidence for a strong intrinsic electric field at or near the interface of microdroplets on the order of ~10^9 V m^{-1}. Such a high electric field was postulated to dissociate hydroxide anion (OH^-) and induce some fraction to be present as ion pairs (16), thereby creating an OH radical and an electron (e^-) at the interface (10, 18). Our experimental evidence supports the hypothesis that OH radicals can spontaneously form at the air–water interface of aerosol and cloud droplets in the dark, without the requirement of any other catalyst or known OH precursors such as Fe(II) cations for Fenton-type reactions. To assess the atmospheric significance of this process, we compared this intrinsic interfacial chemistry with existing pathways known to produce $OH_{(aq)}$.

Fig. 4 shows our experimentally determined interfacial $OH_{(aq)}$ production rates of 10^{-7} to 10^{-6} M s^{-1} for deliquesced submicron aerosols (100 to 300 nm) as well as 5.2 ± 0.7 × 10^{-9} M s^{-1} for microdroplets at a mean diameter of 2.6 μm (*SI Appendix*, Fig. S5*D* and Text S5). The interfacial $OH_{(aq)}$ production rates were compared to the calculated uptake rate from the gas phase under different assumptions for the $OH_{(g)}$ concentration and its mass accommodation coefficient (α), as well as the bulk production rates taken from the literature (*SI Appendix*, Texts S11 and S12). $OH_{(aq)}$ bulk production rates are mainly controlled by the chemical composition and reaction conditions (e.g., photochemistry and dark

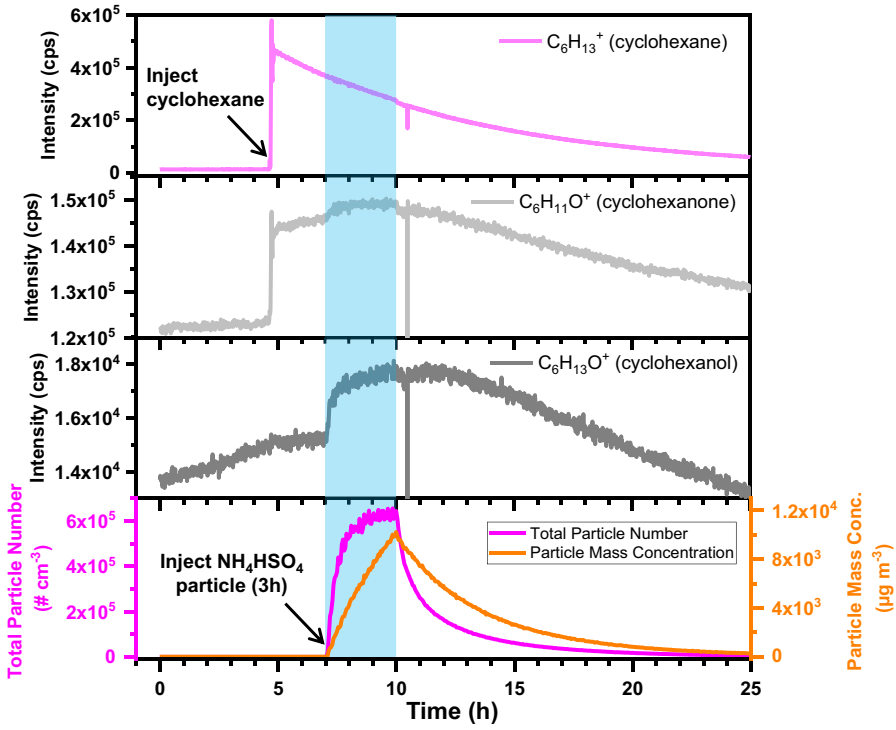

Fig. 3. Dark oxidation of gas-phase species by interfacial OH radicals produced from deliquesced submicron aerosols. Gaseous cyclohexane (~1.1 ppm) was first introduced into the chamber as an $OH_{(g)}$ scavenger, and increasing signals were observed for both cyclohexanone and cyclohexanol in the gas phase (measured by Vocus PTR-ToF-MS) after injecting NH_4HSO_4 aerosol droplets (blue shaded area), suggesting the cyclohexane oxidation chemistry initiated by interfacial OH radicals.

Fenton chemistry) in the bulk (26), varying from type of droplet sample and locations. We realize that $OH_{(aq)}$ bulk production rates can be particle size dependent and may increase as the droplet sizes decrease if the OH-producing solutes are more (41). However, parameterization of this effect is difficult. Therefore, we assume that the literature-derived $OH_{(aq)}$ bulk production rates are independent of droplet size for simplified consideration, which may not accurately reflect realistic conditions but provide an approximate range of 10^{-10} to 10^{-9} M s^{-1}.

The interfacial $OH_{(aq)}$ production rates obtained from our chamber experiments were further extrapolated to different droplet sizes by assuming a simple surface-to-volume dependence following a $radius^{-1}$ trend. As shown in Fig. 4, the interfacial $OH_{(aq)}$ production rate for microdroplets obtained from atomizing experiments closely fitted the lower limit of the extrapolated range, although this rate may be underestimated due to the water vapor dilution effect from the atomizer output. Overall, the interfacial production and uptake rate have comparable OH production rates for small droplets. However, the interfacial pathway dominates for larger droplets, i.e., for the cloud droplet range (5 to 50 μm). During the nighttime, when the gaseous OH concentration is low (i.e., 5×10^4 cm^{-3} as the average nighttime $OH_{(g)}$ (42)), the interfacial pathway dominates across all droplet diameters, suggesting that this is likely the largest aqueous OH source in atmospheric droplets at nighttime.

This comparison indicates that interfacial chemistry may be an important channel for atmospheric multiphase oxidation chemistry. Apart from OH radicals, the spontaneously released electrons likely react with O_2 to form superoxide (O_2^-), which may further form HO_2 and H_2O_2 (**R2**–**R4**). While this spontaneous H_2O_2 formation is still under debate (43), with possible contradictions being explained by the presence or not of suitable electron scavengers (**R2**), we suggest that this interfacial chemistry should be considered in models as it may affect the budget of reactive oxygen species in aerosols, which have been considered to significantly contribute to the oxidative potential of particles, resulting in adverse health effects (6). In contrast to the daytime photochemical OH production, this interfacial mechanism may explain the aqueous oxidation and formation of secondary aerosol observed under high humidity conditions at nighttime (44, 45). Because aerosol and cloud droplets are ubiquitous components of the atmospheric system, our study is therefore regarded as a step toward quantifying the influence of such spontaneous interfacial OH radical production on heterogeneous or multiphase processes, which may provide profound implications on how atmospheric aerosols affect air quality, climate change, and human health. However, more in-depth investigation is still needed to quantitatively assess the contribution of such spontaneous interfacial OH production to heterogeneous chemistry processes such as secondary organic aerosol formation.

In summary, we have provided strong experimental evidence for the spontaneous production of OH radicals at the air–water interface of aerosolized droplets in the dark. This production does not depend on any precursors and correlates with the air–water interfacial area. Some of the interfacial OH can initiate oxidation chemistry of gas-phase compounds and thus may generate gas-phase products. Extrapolation of our observed OH formation rates to atmospheric conditions indicates that this source could be a major but previously unrecognized contributor to the atmospheric aqueous OH formation, particularly in the dark.

Materials and Methods

Chamber Experiment Setup and Experimental Conditions. As shown in *SI Appendix*, Fig. S6, the chamber experiments were performed in a home-built multiphase atmospheric simulation chamber facility (~2 m^3), which was made of a Teflon (fluorinated ethylene propylene) film, fixed as a frame-style cuboid (46, 47). The chamber experimental conditions (experiment ID: E1–E10 and E11–E12) are summarized in *SI Appendix*, Tables S1 and S2. Deliquesced aerosol particles were introduced into the chamber by atomizing different bulk solutions

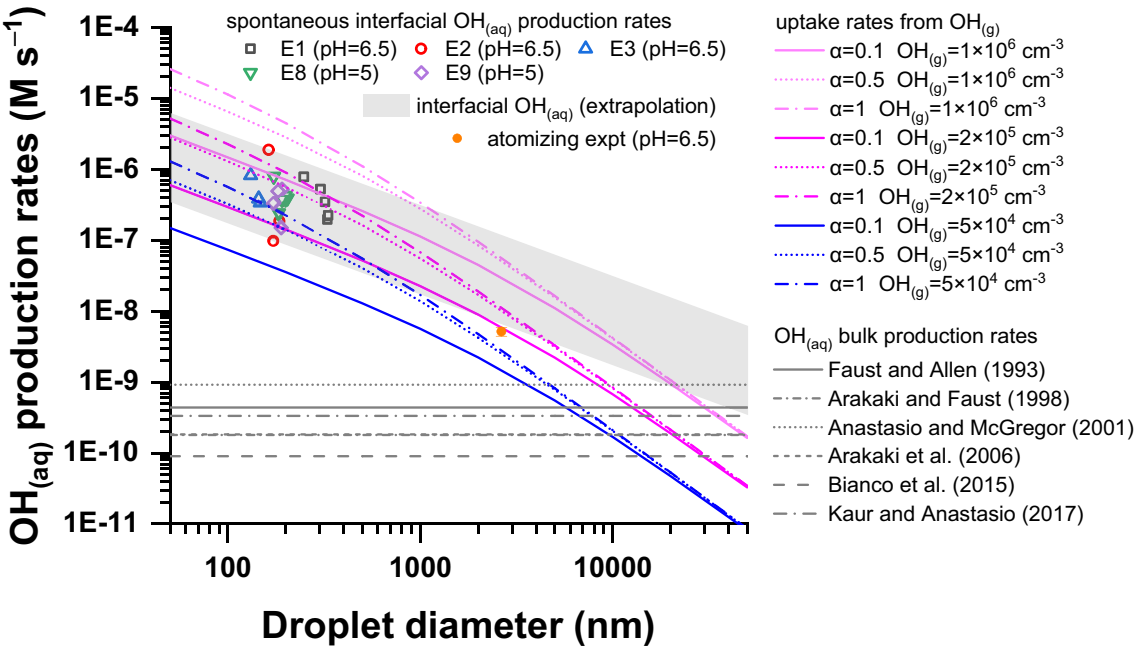

Fig. 4. $OH_{(aq)}$ production rate as a function of droplet size. Open symbols represent interfacial $OH_{(aq)}$ production rates for deliquesced submicron aerosols (at 100 to 300 nm) derived from five chamber experiments (experiment ID: E1, E2, E3, E8, and E9; *SI Appendix*, Table S1), while the orange solid dot represents interfacial $OH_{(aq)}$ production rate for microdroplets (at 2.6 μm) determined from atomizing experiments (*SI Appendix*, Fig. S5*D* and Text S5). TAOH product yield is assumed as 0.315 (33). We assume that the interfacial $OH_{(aq)}$ production rate is proportional to the surface-to-volume ratio, and the extrapolated gray shaded area is represented as its maximum range based on chamber experiments. The OH uptake rates (gas-to-droplet partition) were theoretically calculated (*SI Appendix*, Text S11) by varying mass accommodation coefficients (α = 0.1, 0.5, and 1) and $OH_{(g)}$ concentrations (5×10^4, 2×10^5, and 1×10^6 cm^{-3}). The $OH_{(aq)}$ bulk production rates were extracted from previous literature (*SI Appendix*, Text S12), which collected aerosol, fog, and/or cloud water samples at various locations with purposes of determining the $OH_{(aq)}$ photochemical bulk production rates, and we assume the $OH_{(aq)}$ bulk production rates are mainly determined by its chemical composition but independent with droplet size.

(25 mM NH_4Cl + 1 mM TA) under pressurized pure air (~3 bar) as input gas, and the pH of which was adjusted for some bulk solutions. Some experiments were performed with added gas-phase cyclohexane or a solution-phase OH scavenger (e.g., 1-butanol or adipic acid). Note that we initially tried with 1-butanol as an $OH_{(aq)}$ scavenger in experiment E5, but large amounts of 1-butanol evaporating into the gas phase were observed by a proton transfer reaction time-of-flight mass spectrometer (PTR-ToF-MS; see *SI Appendix*, Text S8) when introducing the aerosol droplet into the chamber. Afterward, we choose adipic acid as an $OH_{(aq)}$ scavenger (in experiments E6 and E7) due to its low volatility and high $OH_{(aq)}$ rate constant (2.0×10^9 M^{-1} s^{-1}, which is comparable to that for TA with $OH_{(aq)}$ at 4.4×10^9 M^{-1} s^{-1}), and there was no detectable gas-phase adipic acid in those experiments. All the chamber experiments were performed in a similar way under room temperature (~23 °C), moderately high relative humidity (RH) (~76%), and dark conditions, except the experiment (E11) with gas-phase cyclohexane under UV irradiation in *SI Appendix*, Fig. S14.

Here, we briefly summarize the chamber experiment procedure. Before starting an experiment, the chamber was continuously flushed with clean air for at least 12 h. The RH in the chamber was increased to ~76% by continuously filling it with a humidified clean airflow (produced by a bubbler). The high RH condition was chosen to maintain the particle in a deliquescent state in the chamber, particularly for NH_4Cl or NH_4HSO_4 aerosol droplets as their efflorescence relative humidity values are much lower than 76% (48). We atomized the fresh bulk solution (typically 25 mM NH_4Cl + 1 mM TA) with a commercial constant output atomizer (TSI 3076) with pure pressurized air to generate TA-containing aerosol droplets and assumed that the chemical components in the atomized aerosol droplets are overall consistent with the bulk solution. The aerosol flow was first passed through a 5-L clean bottle, which was used to trap the large water droplets before entering the chamber. The chamber aerosol number size distribution was monitored by a Scanning Mobility Particle Sizer (TSI 3936), which can also be used to derive the total aerosol number, mass, and volume concentrations. *SI Appendix*, Figs. S7 and S8 show the evolution of particle concentration and size distribution from three typical chamber experiments marked with aerosol droplet injecting and filter sampling periods. The chamber aerosol droplets generally showed a broad size distribution within the submicron range, with a median diameter of 100 to 300 nm. In contrast, the larger water droplets (microdroplets) were mostly lost in the trapping bottle or chamber wall due to their short lifetime. For some experiments, PTR-ToF-MS was employed to monitor the gas-phase volatile organic compounds in the chamber.

The chamber aerosol droplets were collected onto a 47-mm quartz filter (Tissuquartz 2500-QAT-UP, PALL Life Sciences) through a particle sampler with a fixed pumping flow rate of ~5.3 L min^{-1}. Each filter collected the sample for a known duration (usually ~60 min) corresponding to 0.318 m^3 air from the chamber. Note that ~10 L min^{-1} humidified air was continuously supplied to the chamber during the filter sampling period, maintaining a very small positive pressure (~3 Pa) in the chamber to avoid contamination from the room air. After filter collection, the filters were extracted with pure water (*SI Appendix*, Text S6) for subsequent fluorescence analysis, and some samples were also analyzed with offline liquid chromatography (*SI Appendix*, Text S7).

Cleanness of the Performed Experiments. The spontaneous H_2O_2 production from microdroplets by Zare and coworkers (10, 11) has received great attention and debates in very recent years. Fox example, some studies failed to detect this spontaneously generated H_2O_2 and argued that the air–water interface of water microdroplets does not produce H_2O_2 and suspected that H_2O_2 production might be due to ozone contamination (43, 49). However, some newer studies still support this spontaneous H_2O_2 production by very careful and clean experiments (18) and theoretical simulation (19). Nevertheless, one would still suspect that the OH radical formation in our experiments might be due to similar ozone contamination. The pure air we used for different experimental systems was generated by a home-built zero-air generator, in which the output of air compressor is directed to several filter components (ref: DF-0070-ZK, DF-0070-PS, DFM-0070-MIK G1/2, and VARIODRY SP N 0048; Donaldson Company, Inc.). We have carefully checked the purity of the pure air, and no detectable ozone was found by a commercial ozone analyzer (Thermo 49i) across the whole experiment campaign. In addition, by comparing the mist chamber results using purified air vs. synthetic air (80% N_2 + 20% O_2), no significant difference was found as shown in Fig. 1*B* and *SI Appendix*, Fig. S4.

Different types of experiments were performed carefully to avoid any potential contamination. Specifically, all solutions were freshly prepared

using ultrapure water (Elga Purelab Classic, 18.2 MΩ cm) and then used for flat surface experiments (*SI Appendix*, Text S3), mist chamber experiments (*SI Appendix*, Text S4), atomizing experiments (*SI Appendix*, Text S5), or atmospheric simulation chamber on the same day. We intentionally did not use any sonication during solution preparation or filter extraction as it would produce $OH_{(aq)}$ radical in the solution (26). The commercial atomizer was cleaned thoroughly with pure water and ethanol and then baked in an oven (~120 °C) for overnight before starting a new experiment. *SI Appendix*, Fig. S7 shows a blank chamber experiment (performed after a typical TA chamber experiment the next day) that only injects NH_4Cl droplets into the chamber, and no TAOH fluorescence emission spectra were observed from the filter extracts. This indicates that there was no residual TA/TAOH contamination or memory effect in the atomizer after a complete cleaning.

The chemicals we used for preparing bulk TA solutions were in the highest purity grade that were commercially available, such as 99.99% for NH_4Cl and ≥99% for TA (*SI Appendix*, Text S1). In order to test whether there is potential contamination due to the impurity of these chemicals (i.e., transition metals), we pipetted small amount of concentrated TA or TA + NH_4Cl solutions onto the clean filters. These filters were dried under room temperature for several hours and then extracted in the same way as described in *SI Appendix*, Text S6, and no TAOH fluorescence signal was detected from these filter extracts. All these results lead us to conclude that the observed interfacial OH radical formation in our different experimental systems is highly unlikely related to ozone contamination from the purified air or any impurity of the chemicals we used, and it is also not related to uncareful experimental procedures or interference from quartz filter itself.

Data, Materials, and Software Availability. All study data are included in the article and/or *SI Appendix*.

ACKNOWLEDGMENTS. This study was supported by the European Research Council (ERC) under the Horizon 2020 research and innovation program/ERC Grant Agreement 101052601–Spontaneous interfacial oxidant formation as a key driver for aerosol oxidation (SOFA). T.A. and Y.G. acknowledge the financial support from the National Natural Science Foundation of China (42020104001 and 42007192). Y.R. acknowledges partial support by the Israel Science Foundation with grant #928/21. K.L. and C.G. are extremely grateful to D.J. Donaldson, University of Toronto, for critically reading the manuscript and helpful discussion.

Author affiliations: [a]Université Claude Bernard Lyon 1, CNRS, IRCELYON, Villeurbanne F-69626, France; [b]Guangdong Key Laboratory of Environmental Catalysis and Health Risk Control, Guangdong-Hong Kong-Macao Joint Laboratory for Contaminants Exposure and Health, Institute of Environmental Health and Pollution Control, Guangdong University of Technology, Guangzhou 510006, China; [c]Department of Chemistry, University of California, Irvine, CA 92697; and [d]Department of Earth and Planetary Sciences, Weizmann Institute, Rehovot 76100, Israel

1. M. F. Ruiz-Lopez, J. S. Francisco, M. T. C. Martins-Costa, J. M. Anglada, Molecular reactions at aqueous interfaces. *Nat. Rev. Chem.* **4**, 459–475 (2020).
2. C. George, M. Ammann, B. D'Anna, D. J. Donaldson, S. A. Nizkorodov, Heterogeneous photochemistry in the atmosphere. *Chem. Rev.* **115**, 4218–4258 (2015).
3. S. Rossignol *et al.*, Atmospheric photochemistry at a fatty acid-coated air-water interface. *Science* **353**, 699–702 (2016).
4. J. P. Reid, R. M. Sayer, Heterogeneous atmospheric aerosol chemistry: Laboratory studies of chemistry on water droplets. *Chem. Soc. Rev.* **32**, 70–79 (2003).
5. R. J. Huang *et al.*, High secondary aerosol contribution to particulate pollution during haze events in China. *Nature* **514**, 218–222 (2014).
6. M. Shiraiwa *et al.*, Aerosol health effects from molecular to global scales. *Environ. Sci. Technol.* **51**, 13545–13567 (2017).
7. J. H. Seinfeld *et al.*, Improving our fundamental understanding of the role of aerosol-cloud interactions in the climate system. *Proc. Natl. Acad. Sci. U.S.A.* **113**, 5781–5790 (2016).
8. H. Su, Y. Cheng, U. Poschl, New multiphase chemical processes influencing atmospheric aerosols, air quality, and climate in the anthropocene. *Acc. Chem. Res.* **53**, 2034–2043 (2020).
9. Z. Wei, Y. Li, R. G. Cooks, X. Yan, Accelerated reaction kinetics in microdroplets: Overview and recent developments. *Annu. Rev. Phys. Chem.* **71**, 31–51 (2020).
10. J. K. Lee *et al.*, Spontaneous generation of hydrogen peroxide from aqueous microdroplets. *Proc. Natl. Acad. Sci. U.S.A.* **116**, 19294–19298 (2019).
11. J. K. Lee *et al.*, Condensing water vapor to droplets generates hydrogen peroxide. *Proc. Natl. Acad. Sci. U.S.A.* **117**, 30934–30941 (2020).
12. J. K. Lee, D. Samanta, H. G. Nam, R. N. Zare, Micrometer-sized water droplets induce spontaneous reduction. *J. Am. Chem. Soc.* **141**, 10585–10589 (2019).
13. C. Gong *et al.*, Spontaneous reduction-induced degradation of viologen compounds in water microdroplets and its inhibition by host-guest complexation. *J. Am. Chem. Soc.* **144**, 3510–3516 (2022).
14. H. Xiong, J. K. Lee, R. N. Zare, W. Min, Strong electric field observed at the interface of aqueous microdroplets. *J. Phys. Chem. Lett.* **11**, 7423–7428 (2020).
15. H. Hao, I. Leven, T. Head-Gordon, Can electric fields drive chemistry for an aqueous microdroplet? *Nat. Commun.* **13**, 280 (2022).
16. A. I. Kloss, Electron-radical dissociation and the water activation mechanism. *Doklady Akademii Nauk Sssr* **303**, 1403–1407 (1988).
17. C. Xiang, K. M. Papadantonakis, N. S. Lewis, Principles and implementations of electrolysis systems for water splitting. *Mater. Horiz.* **3**, 169–173 (2016).
18. M. A. Mehrgardi, M. Mofidfar, R. N. Zare, Sprayed water microdroplets are able to generate hydrogen peroxide spontaneously. *J. Am. Chem. Soc.* **144**, 7606–7609 (2022).
19. J. P. Heindel, H. Hao, R. A. LaCour, T. Head-Gordon, Spontaneous formation of hydrogen peroxide in water microdroplets. *J. Phys. Chem. Lett.* **13**, 10035–10041 (2022).
20. L. Zhao *et al.*, Sprayed water microdroplets containing dissolved pyridine spontaneously generate pyridyl anions. *Proc. Natl. Acad. Sci.* **119**, e2200991119 (2022).
21. D. Xing *et al.*, Capture of hydroxyl radicals by hydronium cations in water microdroplets. *Angew. Chem. Int. Ed Engl.* **61**, e202207587 (2022).
22. E. A. Pillar-Little, R. C. Camm, M. I. Guzman, Catechol oxidation by ozone and hydroxyl radicals at the air-water interface. *Environ. Sci. Technol.* **48**, 14352–14360 (2014).
23. E. A. Pillar-Little, M. I. Guzman, Oxidation of substituted catechols at the air-water interface: Production of carboxylic acids, quinones, and polyphenols. *Environ. Sci. Technol.* **51**, 4951–4959 (2017).
24. M. S. Rana, M. I. Guzman, Oxidation of phenolic aldehydes by ozone and hydroxyl radicals at the air-water interface. *J. Phys. Chem. A* **124**, 8822–8833 (2020).
25. M. S. Rana, M. I. Guzman, Oxidation of catechols at the air-water interface by nitrate radicals. *Environ. Sci. Technol.* **56**, 15437–15448 (2022).
26. S. Gligorovski, R. Strekowski, S. Barbati, D. Vione, Environmental implications of hydroxyl radicals (•OH). *Chem. Rev.* **115**, 13051–13092 (2015).
27. H. Herrmann, D. Hoffmann, T. Schaefer, P. Brauer, A. Tilgner, Tropospheric aqueous-phase free-radical chemistry: Radical sources, spectra, reaction kinetics and prediction tools. *Chemphyschem* **11**, 3796–3822 (2010).
28. T. Arakaki, B. C. Faust, Sources, sinks, and mechanisms of hydroxyl radical (•OH) photoproduction and consumption in authentic acidic continental cloud waters from whiteface mountain, new york: The role of the Fe(r) (r = II, III) photochemical cycle. *J. Geophys. Res. Atmos.* **103**, 3487–3504 (1998).
29. B. Ervens, Modeling the processing of aerosol and trace gases in clouds and fogs. *Chem. Rev.* **115**, 4157–4198 (2015).
30. B. Ervens, "Progress and problems in modeling chemical processing in cloud droplets and wet aerosol particles" in *Multiphase Environmental Chemistry in the Atmosphere, ACS Symposium Series*, S. W. Hunt, A. Laskin, S. A. Nizkorodov, Eds. (American Chemical Society, 2018), **vol. 1299**, pp. 327–345.
31. E. Pillar-Little, M. Guzman, An overview of dynamic heterogeneous oxidations in the troposphere. *Environments* **5**, 104 (2018).
32. S. E. Page, W. A. Arnold, K. McNeill, Assessing the contribution of free hydroxyl radical in organic matter-sensitized photohydroxylation reactions. *Environ. Sci. Technol.* **45**, 2818–2825 (2011).
33. D. H. Gonzalez, X. M. Kuang, J. A. Scott, G. O. Rocha, S. E. Paulson, Terephthalate probe for hydroxyl radicals: Yield of 2-hydroxyterephthalic acid and transition metal interference. *Anal. Lett.* **51**, 2488–2497 (2018).
34. S. E. Paulson *et al.*, A light-driven burst of hydroxyl radicals dominates oxidation chemistry in newly activated cloud droplets. *Sci. Adv.* **5**, eaav7689 (2019).
35. T. Charbouillot *et al.*, Performance and selectivity of the terephthalic acid probe for OH as a function of temperature, pH and composition of atmospherically relevant aqueous media. *J. Photochem. Photobiol. A Chem.* **222**, 70–76 (2011).
36. H. Herrmann *et al.*, Tropospheric aqueous-phase chemistry: kinetics, mechanisms, and its coupling to a changing gas phase. *Chem. Rev.* **115**, 4259–4334 (2015).
37. H. O. T. Pye *et al.*, The acidity of atmospheric particles and clouds. *Atmos. Chem. Phys.* **20**, 4809–4888 (2020).
38. A. J. Eugene, E. A. Pillar-Little, A. J. Colussi, M. I. Guzman, Enhanced acidity of acetic and pyruvic acids on the surface of water. *Langmuir* **34**, 9307–9313 (2018).
39. L. Wen *et al.*, T- and pH-dependent kinetics of the reactions of ·OH(aq) with glutaric and adipic acid for atmospheric aqueous-phase chemistry. *ACS Earth Space Chem.* **5**, 1854–1864 (2021).
40. M. S. Alam *et al.*, Total radical yields from tropospheric ethene ozonolysis. *Phys. Chem. Chem. Phys.* **13**, 11002–11015 (2011).
41. C. Anastasio, J. T. Newberg, Sources and sinks of hydroxyl radical in sea-salt particles. *J. Geophys. Res. Atmos.* **112**, 10306 (2007).
42. F. Holland, A. Hofzumahaus, J. Schäfer, A. Kraus, H.-W. Pätz, Measurements of OH and HO2 radical concentrations and photolysis frequencies during BERLIOZ. *J. Geophys. Res.* **108**, 8246 (2003).
43. A. Gallo Jr., *et al.*, On the formation of hydrogen peroxide in water microdroplets. *Chem. Sci.* **13**, 2574–2583 (2022).
44. J. Wang *et al.*, Aqueous production of secondary organic aerosol from fossil-fuel emissions in winter beijing haze. *Proc. Natl. Acad. Sci. U.S.A.* **118**, e2022179118 (2021).
45. J. Peng *et al.*, Explosive secondary aerosol formation during severe haze in the north china plain. *Environ. Sci. Technol.* **55**, 2189–2207 (2021).
46. M. Bruggemann *et al.*, Interfacial photochemistry of biogenic surfactants: A major source of abiotic volatile organic compounds. *Faraday Discuss.* **200**, 59–74 (2017).
47. P. A. Alpert *et al.*, Fatty acid surfactant photochemistry results in new particle formation. *Sci. Rep.* **7**, 12693 (2017).
48. C. Peng, L. Chen, M. Tang, A database for deliquescence and efflorescence relative humidities of compounds with atmospheric relevance. *Fundamental Res.* **2**, 578–587 (2022).
49. N. H. Musskopf, A. Gallo Jr., P. Zhang, J. Petry, H. Mishra, The air-water interface of water microdroplets formed by ultrasonication or condensation does not produce H2O2. *J. Phys. Chem. Lett.* **12**, 11422–11429 (2021).